Eur. Phys. J. B **40**, 145–151 (2004)
DOI: 10.1140/epjb/e2004-00253-3

THE EUROPEAN PHYSICAL JOURNAL B

Interpreting remanence isotherms: a Preisach-based study

R.M. Roshko[a] and C. Viddal

Department of Physics and Astronomy, University of Manitoba, Winnipeg MB R3T 2N2, Canada

Received 15 january 2004 / Received in final form 16 April 2004
Published online 12 August 2004 –

Abstract. Numerical simulations of the field dependence of the isothermal remanent moment (IRM) and the thermoremanent moment (TRM) are presented, based on a Preisach formalism which decomposes the free energy landscape into an ensemble of thermally activated, temperature dependent, double well subsystems, each characterized by a dissipation field H_d and a bias field H_s. The simulations show that the TRM approaches saturation much more rapidly than the corresponding IRM and that, as a consequence, the characteristics of the IRM are determined primarily by the distribution of dissipation fields, as defined by the mean field $\bar{H}_d(T)$ and the dispersion $\sigma_d(T)$, while the characteristics of the TRM are determined primarily by a mixture of the mean dissipation field $\bar{H}_d(T)$ and the dispersion of bias fields $\sigma_s(T)$. The simulations also identify a regime $\bar{H}_d \gg \sigma_s$, where the influence of $\bar{H}_d(T)$ on the TRM is negligible, and hence where the TRM and the IRM provide essentially independent scans of the Preisach distribution along the two orthogonal H_s and H_d directions, respectively. The systematics established by the model simulations are exploited to analyze TRM and IRM data from a mixed ferromagnetic perovskite $Ca_{0.4}Sr_{0.6}RuO_3$, and to reconstruct the distribution of characteristic fields H_d and H_s, and its variation with temperature.

PACS. 75.60.Ej Magnetization curves, hysteresis, Barkhausen and related effects – 75.60.-d Domain effects, magnetization curves, and hysteresis

1 Introduction

Magnetic systems which exhibit hysteresis are typically characterized by a free energy G which is an extremely complicated functional of the vector field $\vec{M}(\vec{r})$ which describes the magnitude and direction of the local magnetization vector at all points $\vec{r}$ in the material. The free energy surface possesses a multitude of local minima, maxima, and saddle points, with local minima representing metastable magnetization configurations $\vec{M}_{ms}(\vec{r})$. Much of the complexity derives from natural structural disorder, which ensures that, for a given magnetic field H_a, there will be many different metastable states with the same spatially-averaged magnetization.

However, if a magnetic material exhibits return-point memory [1] (meaning that a field sweep from saturation $\pm H_{a,sat}$ to H_{a1} followed by field cycling from H_{a1} to H_{a2} and back to H_{a1} wipes out memory of the intermediate field reversal to H_{a2} and restores the system to the same state it occupied following the initial sweep to H_{a1}) and congruency [1] (meaning that minor hysteresis loops bounded by the same upper and lower reversal fields H_{aU} and H_{aL} are geometrically congruent provided that the field sequence originated from saturation $\pm H_{a,sat}$), then the system free energy can be decomposed into elementary bistable components [1], each with a double well free energy profile and two characteristic energies, a dissipation barrier W_d and a level splitting W_s, as shown in Figure 1. These energies may be expressed in terms of a characteristic magnetic moment μ, which represents a typical moment reversal associated with a transition between metastable states, and two equivalent fields, a dissipation field H_d and a bias field H_s [2–6]. The conceptual simplicity of the double well structure can be exploited to develop physically transparent and mathematically

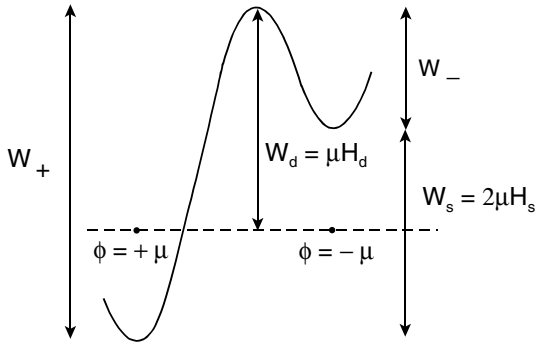

Fig. 1. Double well free energy landscape of an elementary bistable Preisach subsystem with moment μ, states $\pm\mu$, dissipation field H_d, bias field H_s, and excitation barriers W_+ and W_-.

[a] e-mail: roshko@cc.umanitoba.ca

analytical representations of various fundamental states, such as the field cooled (FC) state, the zero field (ZFC) cooled state, the anhysteretic state, and the thermal equilibrium state, and the response of the entire ensemble to an arbitrary sequence of field and temperature excursions can be generated by applying the elegant mathematical algorithms originally developed by Preisach [7].

This paper presents a numerical study of the field dependence of the thermoremanent moment (TRM) and the isothermal remanent moment (IRM), and their relationship to the distribution $p(H_d,\, H_s)$ of equivalent dissipation and bias fields H_d and H_s which characterizes the ensemble of double well potentials. The correlations established by the model simulations are then exploited to analyze TRM and IRM data from a mixed ferromagnetic perovskite $Ca_{0.4}Sr_{0.6}RuO_3$, and to reconstruct the distribution $p(H_d,\, H_s)$ and its variation with temperature.

2 Model simulations

The simulations describe the response of an ensemble of double well potentials (see Fig. 1) with a spectrum of characteristic fields $p(H_d,\, H_s)$ in the form of a product of a lognormal distribution of dissipation fields $f(H_d)$ and a Lorentzian distribution of bias fields $g(H_s)$:

$$\begin{aligned} p(H_d, H_s) &= f(H_d)g(H_s) \\ &= \left(2\pi\sigma_d^2 H_d^2\right)^{-1/2} \exp\left[-\left(\ln\left(H_d/\bar{H}_d\right)\right)^2/2\sigma_d^2\right] \\ &\quad \times (\sigma_s/\pi)\left[H_s^2+\sigma_s^2\right]^{-1}. \end{aligned} \tag{1}$$

Two experimental protocols are considered here: cooling from high temperature in a magnetic field H_a followed by removal of the field, which yields the TRM, and cooling from high temperature in zero field, followed by the application and removal of the field H_a, which yields the IRM.

In a magnetic field H_a, the energies of the two minima in Figure 1 are shifted, and each double well is characterized by a higher energy barrier $W_H = \mu\,(H_d + |H_a - H_s|\,)$ and a lower energy barrier $W_L = \mu\,(H_d - |H_a - H_s|\,)$ [6]. (If W_L is negative, there is only one accessible state.) We assume throughout the discussion that the dissipation barriers $W_d = \mu H_d$ are *not* explicitly dependent on the applied field H_a, so that all excitation barriers W_H and W_L are *linear* functions of H_a. The generalization to nonlinear excitation barriers is addressed in detail in reference [8] in the specific case of systems with Stoner-Wohlfarth-like characteristics. At any temperature T, the maximum energy barrier which can be thermally activated in an experiment with time constant $t_{\rm exp}$ is $W_T = kT\ln(t_{\rm exp}/\tau_0)$, where τ_0^{-1} is a microscopic attempt frequency related to the curvature of the potential well [4–6]. For temperatures where W_T exceeds both W_H and W_L, the subsystem is in thermal equilibrium, the level occupation probabilities are determined by the Boltzmann factor $\exp\left[\pm\mu\,(H_a - H_s)\,/kT\right]$, and the response function is given by

$$M_{eq} = \mu\,\tanh\left[\mu\,(H_a - H_s)\,/kT\right]. \tag{2}$$

When the subsystem is cooled in a field H_a from the equilibrium (superparamagnetic) regime, the subsystem moment is *blocked* at a temperature T_B such that

$$W_H = W_T \tag{3}$$

or

$$\mu\,(H_d + |H_a - H_s|) = kT_B \ln\left(t_{\rm exp}/\tau_0\right). \tag{4}$$

If both W_H and W_L are positive, the level populations are then frozen at $\exp\left[\pm\mu\,(H_a - H_s)\,/kT_B\right]$ and, for all temperatures $T < T_B$, the field cooled (FC) subsystem moment is given by

$$\begin{aligned} M_{\rm FC} &= \mu\,\tanh\left[\mu\,(H_a - H_s)\,/kT_B\right] \\ &= \mu\,\tanh\left[\frac{(H_a - H_s)\,\ln\left(t_{\rm exp}/\tau_0\right)}{H_d + |H_a - H_s|}\right]. \end{aligned} \tag{5}$$

If $W_L < 0$, then $M_{\rm FC} = \pm\mu$.

Removal of the field H_a from the FC state leaves those subsystems with $0 < H_s < H_a$ in an "unstable" configuration, in the sense that the sign of the field cooled moment $M_{\rm FC}$ is *opposite* to the sign of the zero field moment (negative). If the zero field value of the lower energy barrier $W_L = \mu\,(H_d - H_s)$ for these subsystems is either negative or less than the thermal excitation energy W_T, the subsystem will relax to its stable zero field configuration. Subsystems with $W_L > W_T$ will remained *trapped* in their unstable configuration, and will contribute a thermoremanent moment $M_{\rm TRM} = M_{\rm FC}$.

Similarly, when the subsystem is cooled in zero applied field $H_a = 0$, blocking occurs when

$$W_L = \mu\,(H_d + |H_s|) = kT_B \ln\left(t_{\rm exp}/\tau_0\right) \tag{6}$$

which freezes the level populations at $\exp\left[\pm\mu\,(-H_s)\,/kT_B\right]$, and the zero field cooled (ZFC) moment at

$$\begin{aligned} M_{\rm ZFC} &= \mu\,\tanh\left[-\mu H_s/kT_B\right] \\ &= \mu\,\tanh\left[\frac{-H_s \ln\left(t_{\rm exp}/\tau_0\right)}{H_d + |H_s|}\right]. \end{aligned} \tag{7}$$

The application of a positive field H_a induces a positive moment $M_{\rm ZFC+}$ in all subsystems with $0 < H_s < H_a$, for which the lower in-field barrier $W_L = \mu\,(H_d - H_a + H_s)$ is either negative or less than W_T, but leaves subsystems with $W_L > W_T$ trapped in their zero field cooled configuration. Removal of the field restores the zero field negative-moment configuration in equation (7) unless the lower zero field energy barrier $W_L = \mu\,(H_d - H_s)$ exceeds W_T, in which case the subsystem remains trapped in its field-induced positive-moment configuration, and contributes an isothermal remanent moment $M_{\rm IRM} = M_{\rm ZFC+}$.

The expressions (5) and (7) for the moments of the individual Preisach elements $(H_d,\, H_s)$ are specific to the history of field and temperature excursions which define the experimental FC and ZFC protocols, and are thus, in principle, distinguishable from the Preisach configuration which would characterize

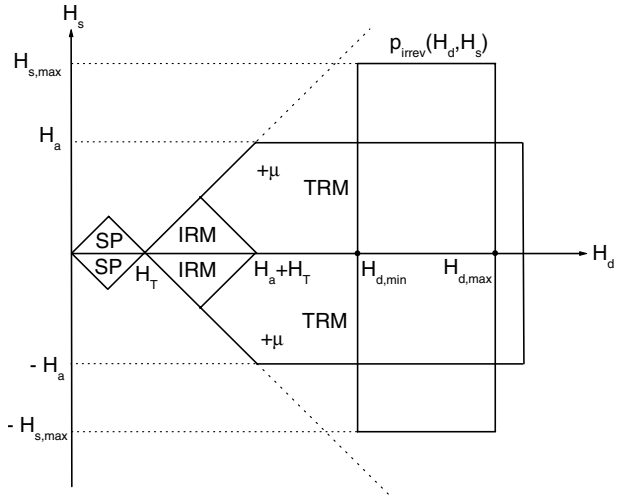

Fig. 2. Preisach representation of the IRM (diamond shaped area) and the TRM (which includes the IRM) obtained by turning off an applied field H_a at temperature T. H_T is the thermal viscosity field. The Preisach IRM and TRM subsystems are all in their $+\mu$ state, and those in the region labelled SP are in thermal equilibrium and respond superparamagnetically. The rectangular area labelled $p_{\rm irrev}(H_d,\, H_s)$ represents the boundaries of an "ideal" Preisach density for which the TRM depends only on the distribution of bias fields $g(H_s)$.

the isothermal anhysteretic magnetizing (AHM) process, which is a history-independent process performed by field cycling with incrementally decreasing amplitude from positive saturation at a fixed temperature. On the other hand, for level splittings such that $|H_a - H_s| \geq 2H_d/\ln(t_{\rm exp}/\tau_0) \sim H_d/10$ (for typical experimental times $t_{\rm exp} \sim 10^2$ s), then $\tanh(x) \cong 1$, and all but a small fraction of the Preisach moments are effectively saturated at $\pm\mu(T)$, so that the distinction between the model FC and AHM configurations is quite subtle.

The FC and ZFC processes are *not isothermal* and, consequently, the Preisach density is expected to evolve continuously during cooling. Given the details of the growth of the individual Preisach elements with temperature, equations (5) and (7) could, in principle, be modified to reflect the specific thermal history of blocking and unblocking events of each element. However, in the absence of such detailed knowledge, a priori, regarding the thermal development of the free energy landscape, we adopt equations (5) and (7) as working definitions of the FC and ZFC moments, and we assume throughout that these moments are *insensitive* to the precise manner in which the Preisach density evolves with temperature.

The thermoremanent state and the isothermal remanent state of an ensemble of double well subsystems obtained by removing a field H_a at temperature T are conveniently summarized by the Preisach diagram in Figure 2, which shows the state of every subsystem as a function of its field coordinates $(H_d,\, H_s)$. In general, the distribution $p(H_d,\, H_s)$ occupies the entire half-plane $H_d > 0$. The total system moment is obtained by integrating over the entire Preisach plane:

$$M(H_a,T) = \int_0^{\infty} dH_d \int_{-\infty}^{+\infty} dH_s\, p(H_d,H_s,T)\, \phi(H_d,H_s,H_a,T) \tag{8}$$

where $\phi\,(H_d,H_s,H_a,T)$ is the state of the subsystem with characteristic fields $(H_d,\, H_s)$. The IRM is obtained by integrating only over the diamond shaped area in Figure 2 labelled IRM, while the TRM is obtained by integrating over the entire area labelled TRM, which includes the IRM. Following the earlier discussion, the remanent state of all the IRM and TRM subsystems is assumed to be $+\mu(T)$. Subsystems in the region labelled SP are superparamagnetic and hence in thermal equilibrium.

One of the primary objectives of a data analysis based on the double well Preisach formalism is the determination of the distribution function $p(H_d,\, H_s)$. In principle, this information is encoded most directly in the field dependence of the IRM and the TRM, although the contributions of the individual H_d and H_s distributions tend to be mixed together due to the presence of the diagonal boundaries on the IRM and the TRM in Figure 2 at $H_d = \pm H_s + W_T/\mu$ and at $H_d = \pm H_s + H_a + W_T/\mu$. However, if the Preisach density $p(H_d,\, H_s)$ is bounded in such a way that the minimum dissipation field $H_{d,min}$, reduced by the effective thermal fluctuation field $H_T = W_T/\mu$, exceeds the maximum bias field $H_{s,max}$ (that is, $H_{d,\rm min} > H_{s,\rm max} + W_T/\mu$), as illustrated by the rectangular distribution labelled $p_{\rm irrev}\,(H_d,\, H_s)$ in Figure 2, then the field dependence of the TRM is determined exclusively by the characteristics of the bias field distribution through the dispersion σ_s, independent of the distribution of dissipation fields. Real distributions are not expected to exhibit abrupt cutoffs, so numerical simulations of the TRM and the IRM were performed with the smooth distributions in equation (1) in order to study the effects of the three parameters $\bar{H}_d$, σ_d, and σ_s individually. These simulations are summarized in Figures 3 through 8.

Figures 3 through 6 illustrate the influence of the distribution of dissipation fields $f(H_d)$ on the field dependence of the TRM and the IRM, for a fixed distribution of bias fields with $\sigma_s = 0.1$. All curves have been normalized to the corresponding saturation remanence. Figures 3 and 4 show the effect of varying the median coercive field $\bar{H}_d$ when thermal fluctuations are entirely absent $(W_T = 0)$, and when the variations in $\bar{H}_d$ are driven entirely by thermal fluctuations through the magnetic viscosity field $H_T = W_T/\mu$, respectively. In both cases, a decrease in $\bar{H}_d$ displaces the IRM towards lower applied fields H_a and induces the TRM to saturate more rapidly. Figures 5 and 6 show the effect of variations in the dispersion of dissipation fields σ_d in the absence of thermal fluctuations $(W_T = 0)$, when $\bar{H}_d \gg \sigma_s$ and when $\bar{H}_d \sim \sigma_s$, respectively. Variations in σ_d clearly have a significant impact on the curvature of the IRM, but a comparatively minor influence on the curvature of the TRM, although the latter becomes progressively more noticeable as $\bar{H}_d \to \sigma_s$, with increases in σ_d delaying the approach to saturation.

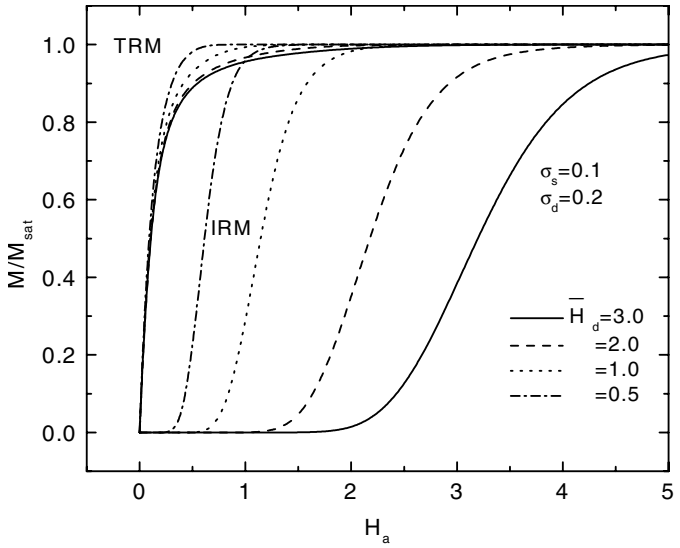

Fig. 3. Preisach simulations of the field dependence of the TRM and the IRM which illustrate the dependence on the mean dissipation field $\bar{H}_d$, for fixed dispersions $\sigma_d = 0.2$ and $\sigma_s = 0.1$.

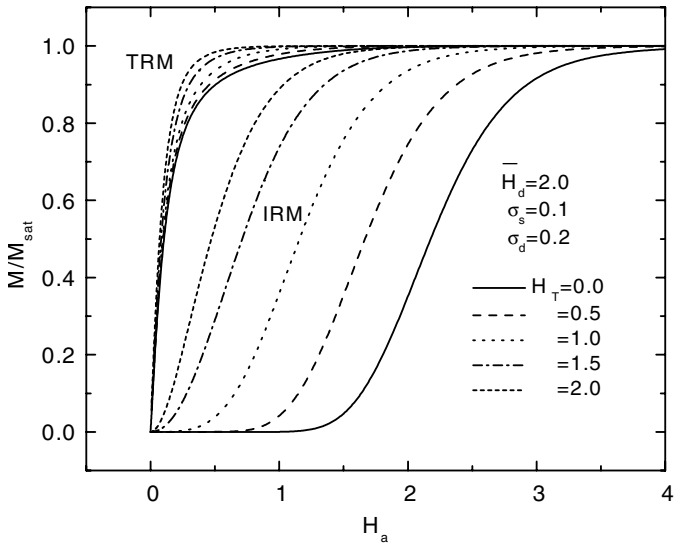

Fig. 4. Preisach simulations of the field dependence of the TRM and IRM which illustrate the dependence on the thermal viscosity field H_T for a fixed Preisach distribution with $\bar{H}_d = 2.0$, $\sigma_d = 0.2$, $\sigma_s = 0.1$.

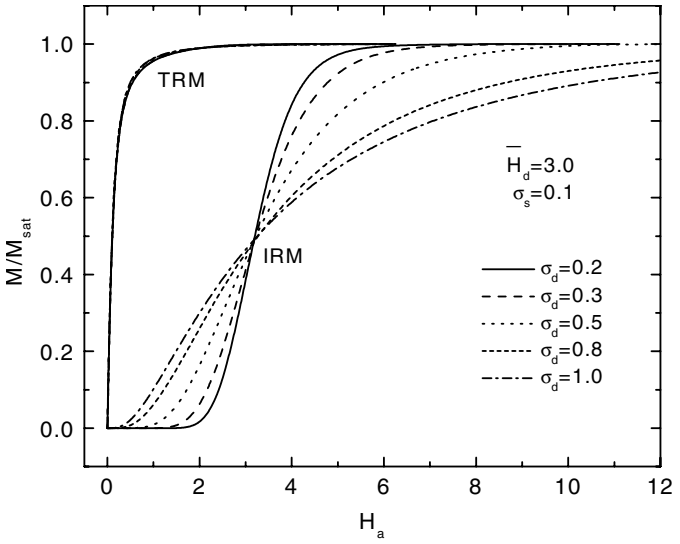

Fig. 5. Preisach simulations of the field dependence of the TRM and IRM which illustrate the dependence on the dispersion of dissipation fields σ_d for fixed $\bar{H}_d = 3.0$ and $\sigma_s = 0.1$.

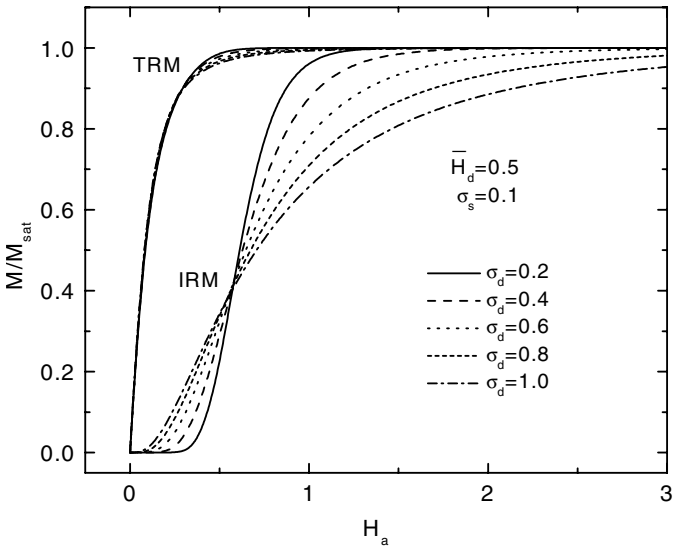

Fig. 6. Preisach simulations of the field dependence of the TRM and IRM which illustrate the dependence on the dispersion of dissipation fields σ_d for fixed $\bar{H}_d = 0.5$ and $\sigma_s = 0.1$.

From Figures 3 through 6, it is apparent that, when $\bar{H}_d \gg \sigma_s$, the TRM is essentially independent of the characteristics of the distribution of dissipation fields $f(H_d)$. In this limit, the field dependence of the TRM yields an essentially undistorted image of the distribution of bias fields $g(H_s)$ or, more precisely, its integral:

$$M_{\mathrm{TRM}}(H_a) \sim \int_0^{H_a} g(H_s)\, dH_s. \tag{9}$$

As the distribution $g(H_s)$ becomes narrower, equation (9) predicts that the TRM will approach saturation progressively more rapidly, and this is indeed confirmed by the simulations in Figure 7, which show the dependence of the TRM and the IRM on the dispersion of bias fields σ_s when $\bar{H}_d \gg \sigma_s$. In this limit then, the TRM and the IRM provide essentially "independent" scans of the Preisach distribution $p(H_d, H_s)$ along the two orthogonal H_d and H_s directions in the Preisach plane, in the sense that once the dispersion σ_s has been identified from measurements of the TRM, the dispersion σ_d can be identified independently from measurements of the IRM.

As $\bar{H}_d \to \sigma_s$, the influence of the diagonal boundaries in the Preisach representation of the TRM in Figure 2 becomes progressively more evident, and the field dependence of the TRM is determined jointly by the

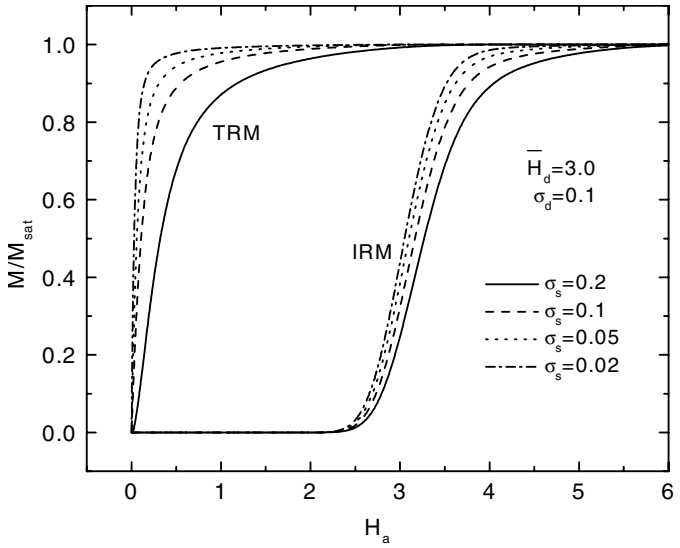

Fig. 7. Preisach simulations of the field dependence of the TRM and IRM which illustrate the dependence on the dispersion of bias fields σ_s for fixed $\bar{H}_d = 3.0$ and $\sigma_d = 0.1$.

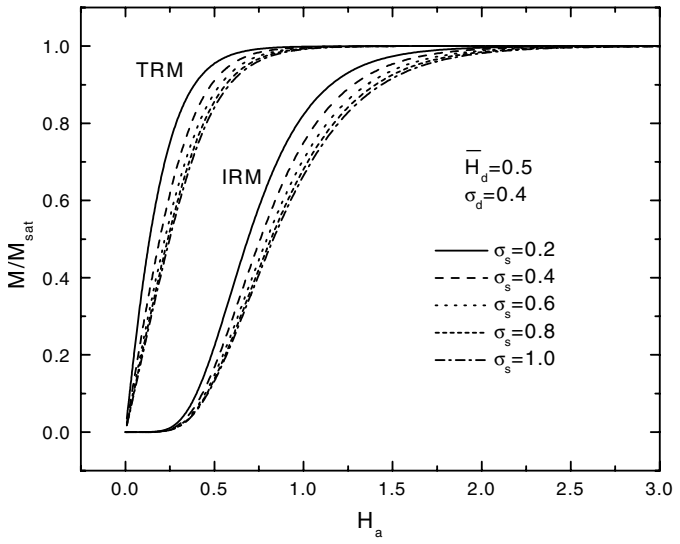

Fig. 8. Preisach simulations of the field dependence of the TRM and IRM which illustrate the dependence on the dispersion of bias fields σ_s for fixed $\bar{H}_d = 0.5$ and $\sigma_d = 0.4$.

characteristics of both $g(H_s)$ and $f(H_d)$. Since the parameter $\bar{H}_d$ is essentially fixed experimentally by the measured remanent coercive field H_{cr}, the analysis of the measured TRM reduces to identifying the two dispersions σ_d and σ_s. In this regard, it is important to note that, even in the limit $\bar{H}_d \to \sigma_s$, the TRM tends to be significantly more sensitive to variations in σ_s than to variations in σ_d, as can be seen by comparing Figure 8, which illustrates the dependence of the TRM and the IRM on σ_s for $\bar{H}_d = 0.5$, with Figure 6.

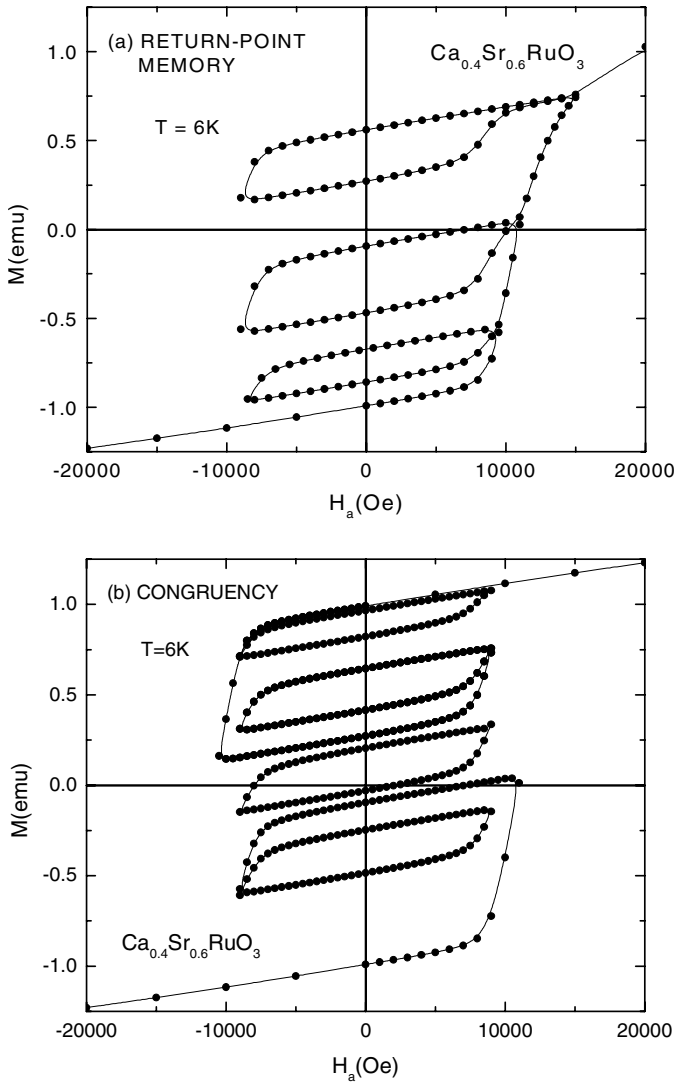

Fig. 9. Experimental tests of the necessary and sufficient conditions for double well decomposition of (a) return-point memory and (b) congruency, for $Ca_{0.4}Sr_{0.6}RuO_3$ at $T = 6$ K.

3 An analysis of remanence isotherms for a ferromagnetic perovskite

In this section, we present a Preisach-based analysis of remanence data for a mixed ferromagnetic perovskite $Ca_{0.4}Sr_{0.6}RuO_3$ with a critical temperature $T_C = 75$ K. In order to assess the validity of the double well decomposition hypothesis for this particular material, experimental tests of return-point memory and congruency were conducted, and some of these are shown in Figures 9a and b, respectively. Within experimental accuracy (limited primarily by the nonreproducibility of the applied field due to hysteresis in the superconducting magnet), the criterion of return-point memory is consistently satisfied for all minor loops which originate and terminate on the major hysteresis loop. The criterion of geometrical congruency of minor loops bounded by the same reversal fields is satisfied for vertical loop displacements which span virtually

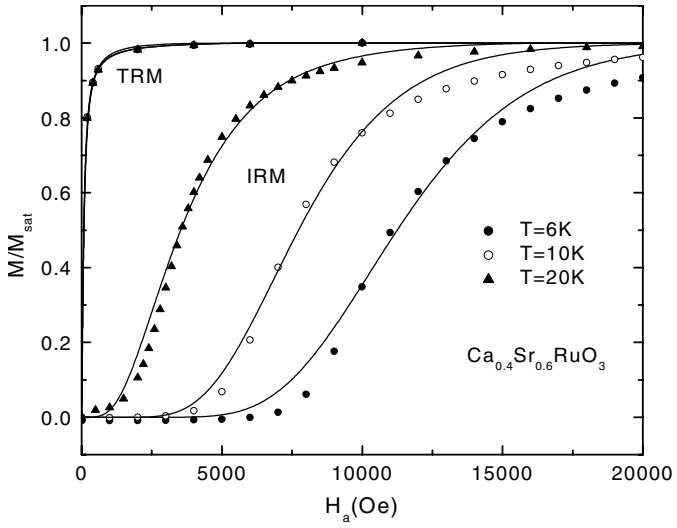

Fig. 10. Measurements (discrete points) of the TRM and the IRM for $Ca_{0.4}Sr_{0.6}RuO_3$ for temperatures $T \leq 20$ K, and Preisach simulations (solid curves).

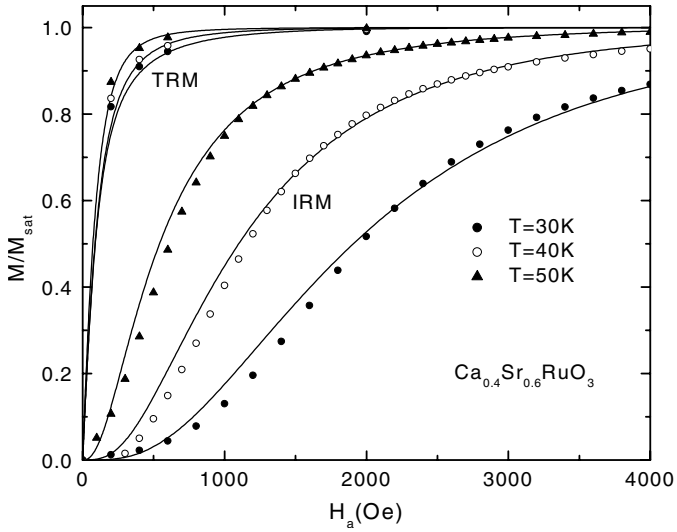

Fig. 11. Measurements (discrete points) of the TRM and the IRM for $Ca_{0.4}Sr_{0.6}RuO_3$ for temperatures $T \geq 30$ K, and Preisach simulations (solid curves).

the entire height of the major hysteresis loop, although violations in the form of a loss of vertical amplitude become progressively more apparent as the minor loops approach the upper and lower branches of the major loop. While the implications of these violations, which may be symptomatic of mean-field effects [2,3] on a spatial scale which is much longer than that of the individual Barkhausen events, are difficult to quantify at this stage, the behaviour observed in Figure 9 nevertheless lends considerable credibility to the double well hypothesis as an interpretive tool with physical substance.

Figures 10 and 11 show measurements (discrete points) of the field dependence of the TRM and the IRM, normalized to saturation, at several representative temperatures T which span the ordered phase. Figure 10 contains remanence data for $T \leq 20$ K for which changes in temperature induce significant changes in the measured remanent coercive field H_{cr} and in the IRM isotherms, but no detectable changes in the TRM, all of which are coincident within experimental accuracy. The solid curves are Preisach simulations of the TRM and IRM generated with the product distribution in equation (1). The fitting protocol involved iteration between the two data sets as follows. An initial fit to a given TRM was performed first by assuming a very narrow distribution of dissipation fields with $\bar{H}_d = H_{cr}$ and $\sigma_d = 0.05$, and by varying only the dispersion of bias fields σ_s. This value of σ_s was then used to generate a fit to the corresponding IRM isotherm by varying only the dispersion of dissipation fields σ_d. The latter value of σ_d was then used to update the TRM fit. For $T \leq 20$ K, this procedure converged in one iteration, as expected, confirming that the TRM in this regime is indeed rigorously independent of the distribution of dissipation fields, and represents an undistorted image of the distribution of bias fields. (Attempts to incorporate mean field effects [9,10] into the distribution of bias fields consistently yielded a vanishingly small mean field parameter, within experimental uncertainty.)

Figure 11 shows remanence data obtained at higher temperatures $T \geq 30$ K. In this regime, systematic changes in the IRM with temperature are accompanied by similar systematic changes in the TRM, specifically, a tendency to approach saturation progressively more rapidly as the system is warmed toward the critical temperature T_C. According to the model simulations in Section 2, such behaviour is symptomatic of either the penetration of the dissipation field distribution into the region to the left of the diagonal boundaries in Figure 2, or the collapse of the bias field distribution, or a combination of these. The solid curves in Figure 10 were obtained by following the same iterative fitting protocol described above and, as before, a single iteration was sufficient to establish the two dispersions σ_s and σ_d. The simulations show that for all temperatures $T \leq 50$ K, the systematic changes observed in the TRM with temperature originate exclusively from the collapse of the distribution of dissipation barriers, specifically from the temperature dependence of the mean dissipation field $\bar{H}_d(T)$. However, the fits to the highest temperature data ($T = 60$ K) measured here clearly suggest that, close to T_C, the collapse of the distribution of dissipation fields alone is insufficient to replicate the evolution of the TRM with temperature, and must be supplemented by the collapse of the distribution of bias fields. The temperature dependences of the two Preisach dispersions are summarized in Figure 12. We point out that, although the current analysis is focussed exclusively on the properties of the irreversible component of the magnetic response, it is possible to replicate the in-field response of the perovskite as well by supplementing the irreversible Preisach density in equation (1) with a reversible density $p_{rev}(H_s) = (\lambda/2)\exp(-\lambda\,|H_s|\,)$, which describes a population of Preisach elements with vanishing dissipation barriers, confined exclusively to the H_s-axis.

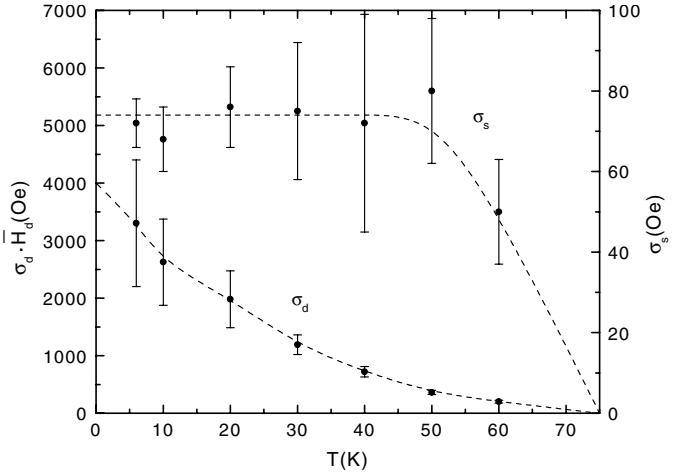

Fig. 12. Temperature dependence of the dispersion of bias fields σ_s and the dispersion of dissipation fields σ_d obtained from the Preisach simulations in Figures 10 and 11. (Dashed lines are guides to the eye.)

4 Summary

Although measurements of the thermoremanent moment and the isothermal remanent moment are a standard component of the experimental characterization of any magnetic material which exhibits magnetic order, their significance as complementary probes of the spectrum of metastable state excitation energies is not widely appreciated. This paper presents numerical simulations of the TRM and the IRM based on the Preisach formalism, which hypothesizes a decomposition of the micromagnetic free energy into double well subsystems, characterized individually by a dissipation energy and a stored energy, and collectively by a distribution of these energies. The strength of the formalism resides in its ability to simulate the magnetic response to an arbitrary sequence of field and temperature excursions, and to relate the principal structural features of the response, and their systematic variation with field and temperature, to the two characteristic energies which are fundamental to all Barkhausen instabilities, regardless of their specific physical origin (wall pinning, wall nucleation, moment rotation, ...).

The numerical simulations show that the TRM is sensitive primarily to variations in the median dissipation field $\bar{H}_d(T)$ and in the dispersion of bias fields $\sigma_s(T)$, while the IRM is sensitive primarily to the characteristics of the distribution of dissipation fields, and hence to variations in $\bar{H}_d(T)$ and in the dispersion $\sigma_d(T)$. Furthermore, the simulations identify a regime $\bar{H}_d(T) \gg \sigma_s(T)$ where the TRM is essentially independent of the distribution of dissipation barriers, and thus provides a virtually undistorted scan along the axis of bias fields H_s in the Preisach plane. The experimental signature of this regime

Table 1. Preisach distribution parameters for $Ca_{0.4}Sr_{0.6}RuO_3$.

T (K)	$\bar{H}_d$ (Oe)	$\sigma_d \bar{H}_d$ (Oe)	σ_s (Oe)
6	11000 ± 100	3300 ± 1100	72 ± 6
10	7500 ± 100	2630 ± 750	68 ± 8
20	3300 ± 50	1980 ± 495	76 ± 10
30	1700 ± 50	1190 ± 170	75 ± 17
40	900 ± 50	720 ± 90	72 ± 27
50	360 ± 30	360 ± 36	80 ± 18
60	250 ±20	200 ±25	50 ± 13

is a measured TRM which reaches saturation in applied fields where the corresponding IRM isotherm is still negligible. Thus, from fits to experimental IRM and TRM data, acquired over a sufficiently wide range of temperatures, it is possible to reconstruct the thermal evolution of the spectrum of metastable state free energy barriers throughout the entire hysteretic regime, and even to distinguish the effects of intrinsic barrier growth from those related to thermal overbarrier activation. In the specific case of the ferromagnetic perovskite analyzed here, thermal fluctuations are negligible throughout most of the ordered phase, and the temperature dependence of the magnetic response is almost exclusively a manifestation of explicit barrier growth, which ultimately originates from the temperature dependence of material parameters like the crystalline anisotropy constants.

The complementary relationship between the IRM and the TRM with respect to the characteristic energies W_d and W_s, and specifically the existence of a limit where the TRM depends exclusively on the distribution of double well level splittings W_s, may prove to be of particular value in the characterization of interaction effects in systems of fine particles, where the level bias most likely originates from the magnetostatic coupling between individual particles or between strongly correlated clusters of particles.

References

1. I.D. Mayergoyz, Phys. Rev. Lett. **56**, 1518 (1986)
2. G. Bertotti, *Hysteresis in Magnetism* (Academic Press, 1998)
3. E. Della Torre, *Magnetic Hysteresis* (IEEE Press, 1999)
4. J. Souletie, J. Phys. France **44**, 1095 (1983)
5. J.J. Prejean, J. Souletie, J. Phys. France **41**, 1335 (1980)
6. T. Song, R.M. Roshko, E.D. Dahlberg, J. Phys.: Condens. Matter **13**, 3443 (2001)
7. F. Preisach, Z. Phys. **94**, 277 (1935)
8. A. Stancu, L. Spinu, IEEE Trans. Magn. **34**, 3867 (1998)
9. E. Della Torre, IEEE Trans. Audio Electroacoust. **14**, 86 (1966)
10. C. Papusoi, A. Stancu, IEEE Trans. Magn. **29**, 77 (1993)